

# HITTITE JOURNAL OF SCIENCE AND ENGINEERING

e-ISSN: 2148-4171  
Volume: 11 • Number: 3  
September 2024

## Investigation of the Defect Effects on the Load-Carrying Capacity of Butt Joints: A Numerical Study

Hamza Taş 

Manisa Celal Bayar University, Hasan Ferdi Turgutlu Faculty of Technology, Department of Mechanical Engineering, 45400, Manisa, Türkiye.

### Corresponding Author

Hamza Taş

E-mail: hamza.tas36@gmail.com Phone: +90 236 314 1010

RORID: <https://ror.org/053f2w588>

### Article Information

Article Type: Research Article

Doi: <https://doi.org/10.17350/HJSE19030000337>

Received: 06.04.2024

Accepted: 05.07.2024

Published: 30.09.2024

### Cite As

Taş, H. Investigation of the Defect Effects on the Load-Carrying Capacity of Butt Joints: A Numerical Study. Hittite J Sci Eng. 2024;11(3):105-113.

**Peer Review:** Evaluated by independent reviewers working in at least two different institutions appointed by the field editor.

**Ethical Statement:** Not available.

**Plagiarism Checks:** Yes - iThenticate

**Conflict of Interest:** Authors approve that to the best of their knowledge, there is not any conflict of interest or common interest with an institution/organization or a person that may affect the review process of the paper.

### CRedit AUTHOR STATEMENT

**Hamza Taş:** Conceptualization, Investigation, Methodology, Validation, Visualization, Writing- original draft,

**Copyright & License:** Authors publishing with the journal retain the copyright of their work licensed under CC BY-NC 4.

# Investigation of the Defect Effects on the Load-Carrying Capacity of Butt Joints: A Numerical Study

Hamza Taş

Manisa Celal Bayar University, Hasan Ferdi Turgutlu Faculty of Technology, Department of Mechanical Engineering, 45400, Manisa, Türkiye.

## Abstract

Determining the behavior of joints under a specific load and estimating the damage potential is essential for ensuring the durability of joints in engineering structures. Defects might occur at the adhesive layer, which causes a reduction in the durability of joints. This work aims to examine the effects of the defect presence, defect volume fraction, defect position, and random distribution of defects at the adhesive layer on the durability of the butt joint. A finite element (FE) model of the butt joint was constructed using the commercially available FE software Abaqus/Standard. The validation of the FE model was conducted by comparing its results with experimental finding reported in existing literature. Numerical and experimental results showed strong agreement, with relative errors of 2.46% and 2.95% at peak force and displacement at peak force, respectively. Defect presence significantly influences the durability of the butt joint. Defect volume fraction and defect location are the dominant parameters affecting the durability of the butt joint. The square defects at the center of the bonding layer, with volume fractions of 0.05, 0.10, and 0.15, lowers the peak force by 5.08%, 10.56%, and 15.73%, respectively. When the defect is positioned at the center of the bonding layer, adhesive failure starts at the edges of the defects. However, relocating the defect from the center to the left or upper side of the bonding layer results in adhesive failure initiation at the corresponding edges of the adhesive. Random defect distribution in the adhesive layer doesn't affect joint durability.

**Keywords:** Finite element analysis, Butt joint, Adhesive, Defect, Cohesive zone model

## INTRODUCTION

In the last eighty years, the use of adhesively bonded joints has grown due to their advantages over the traditional mechanical fasteners, welding, and brazing [1–4]. Conventional joining techniques including bolting and riveting introduce stress concentration around the application area, which severely impairs the mechanical properties of the joints. Besides, mechanical fasteners can raise the weight of the structure. Adhesively bonded joints could potentially overcome these limitations [5,6]. The key benefits of adhesively bonded joints include uniform stress distribution, cost effectiveness, no need for machining, milling, or forming operations, good strength to weight ratio and high fatigue resistance [7–10]. However, considering their manufacturing sensitivity, adhesively bonded joints are susceptible to defects [3]. Every manufacturing process inherently results in some defects because producing defect-free joints, despite strict controls, is nearly impossible. Entrapped air, dirt, foreign objects, and grease may cause defects in the bonded region. Since load cannot be transferred through these defects, stress concentrations occur around these defects [11]. Hence, it is essential to comprehend the effects of defects in the bonded region on the joint durability.

Many research have been conducted to investigate the effects of defect types [3,12–14], locations [3,11,14–17], shapes [8,15], sizes [8,12,14,16–18], and numbers [11,15,17] on joint strength. Geleta et al. [3] conducted experimental tests and finite element analysis (FEA) for inclined joints. Based on the experimental test results, they incorporated the potential production defect locations and types in the FE model. The results showed that defect types and locations play a crucial role on the joint strength. They further determined that the FE results align well with the experimental findings. Xu and Wei [14] considered three defect types: local debonding, weak bonding, and void. The outcomes of the FEA also revealed that joint strength is significantly influenced by the presence of different types of defects. Jamal-Omidi and Mohammadi Suki [12] considered two different types of defects: void modeled as local delamination in varying dimensions, and locally insufficient bonding characterized as an alteration in the properties of adhesive. The results indicated that defects adversely influence the joint durability. Nevertheless, defect existence in the bonding layer does not change stress field in adherends. Luo et al. [13] worked the influences of the

different kinds of flaws (core material flaw, radius floating of the fillet, and debonding defects) on the strength of composite T-joints under bending load through experiments and numerical analysis. They used cohesive elements to simulate the delamination of interface. The outcomes demonstrated that the types of flaws have no influence on the T-joint failure mode. However, they have a notable impact on the T-joint strength. In addition, it has been noted that the most dangerous type of flaw is the debonding defect in the arc region. Fame et al. [17] examined the failure sensitivity of adhesively bonded GFRP joints under uniaxial tensile loading utilizing FE method, while considering flaws at varied positions, numbers, and sizes in the bondline. According to the findings of the finite element analysis, bondline defects cause an increment in out-of-plane displacement of adherends as well as maximum shear and peel stresses at the edges of adhesive. Areas close to the defects also showed high stress concentrations. Heidarpour et al. [8] conducted an experimental study to examine the impacts of shape and size of 2D and 3D flaws on the adhesively bonded single lap joint (SLJ) durability. The findings revealed that for the joint with 3D defects, joint strength drops approximately linearly with the rise of defect area. However, reduction in joint durability for the joint with 2D defect is non-linear. It is also concluded that whereas 2D circular defects result in a lesser strength drop, 2D triangular and square defects cause similar strength reductions. Additionally, compared to 3D circular and square flaws, the strength drop for 3D triangular flaws is higher. Elhannani et al. [15] analyzed the effects of shape, position and number of bonding flaws on the shear stress distribution in the overlap area. Numerical analyzes showed that bonding defects adversely affect the shear stress distribution and that maximum stresses constantly occur at the adhesive edge, without considering the defect size. Dai et al. [16] focused on developing a theoretical model for resolving the multi-failed mechanical problem of an adhesively bonded joint with/without interfacial flaws, and examining the effects of interfacial flaws and hygrothermal conditions on the stress distribution. The results revealed that the effect of the change in defect length is more significant than the effect of defect depth in variations of interfacial stress. Moreover, defects close the edges of the overlap creates a greater risk to the joint. Ribeiro et al. [19] conducted a numerical and experimental investigation into the SLJs with flaws positioned at the center of the adhesive layer for various adhesives and

bonding lengths. According to the findings, the joints bonded with the adhesive 7752 are more influenced by the existence of center-positioned defects in the bonding layer than those bonded with the adhesive AV138.

The existing studies investigating the impact of defect presence, defect volume fraction, defect location, and defect random distribution on the load-carrying capacity of joints, particularly butt joints where normal stress in the adhesive is dominant, remain insufficient. Meanwhile, research efforts predominantly focus on assessing the influence of flaws within the bonding layer specifically for single/double lap joints, T-joints, and inclined joints. This study aims to address the literature gap by primarily investigating the impact of defects within the bonding layer on the load-bearing capacity of butt joints. A three-dimensional FE model was constructed using Abaqus/Standard to investigate the response of the butt joint with/without defect in the bonding layer under uniaxial tensile loading conditions, with a specific emphasis on cohesive failure in the adhesive layer. The accuracy of the numerical model was validated through a comparison with the experimental findings of Ref. [20]. The investigation encompasses an analysis of the effects of defect presence, defect volume fraction, defect position, and random distribution of flaws in the bonding layer on the load-bearing capacity of the butt joint.

**NUMERICAL STUDY**

In the present study, finite element analysis (FEA) of adhesively bonded butt joints were carried out by using a commercially available FEA software Abaqus/Standard. The 3-D geometric model of butt joint and its dimensions are shown in Fig. 1. The adherend dimensions are 100 mm in length, 25 mm in width, and 5 mm in thickness, while the adhesive layer has a thickness of 0.18 mm. The adherends and adhesive were considered as AA2024-T3 aluminum alloy and DP460 epoxy adhesive. The selection of adherend and adhesive materials was based on practical engineering applications [21]. DP460 adhesive is utilized for adhering metal, porcelain, glass, and a variety of composite materials together [22]. The mechanical characteristics of adherend and adhesive used in this study are presented in Table 1. Despite the non-linear behavior of the AA2024-T3 aluminum alloy, adherends were modeled as a linear-elastic material. Because, as can be seen in the following sections, the maximum strain value of aluminum is still in the elastic region when the adhesive fails.

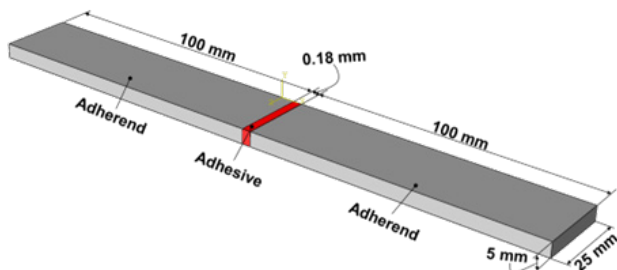


Figure 1 3D geometric model of butt joint (not scaled)

**Table 1** Mechanical properties of AA2024-T3 aluminum alloy and DP460 epoxy adhesive [20]

	AA2024-T3 aluminum alloy	DP460 epoxy adhesive
Young's modulus (MPa)	72400±530	2077±47
Poisson's ratio	0.33	0.38
Ultimate tensile strength (MPa)	482±12	44.6±1.2
Ultimate tensile strain (mm/mm)	0.1587	0.0428

The constructed mesh and applied boundary conditions are presented in Fig. 2. The adherends were modeled using 8-nodes linear hex elements (C3D8R) while adhesive layer was meshed with 8-nodes three-dimensional cohesive elements (COH3D8). The adhesive layer's mesh comprised fine elements, whereas coarse elements constituted the mesh of the adherends. 0.6×0.6×0.6 mm<sup>3</sup> and 0.2×0.2×0.2 mm<sup>3</sup> element dimensions were taken into consideration for adherends and adhesive, respectively. Besides, it is critical to emphasize that the adhesive layer was modeled as a single layer of cohesive element through the thickness. In the opposite case, the calculation doesn't converge [9,23–25]. The surface-to-surface tie constraint was employed to tie adherend and adhesive surfaces with differing mesh structures. As for the boundary conditions, the adhesively bonded butt joint was fixed in all directions at one end, while for the other end, it was fixed in all directions except the x-direction, and a 0.15 mm uniform displacement boundary condition in the x-direction was defined.

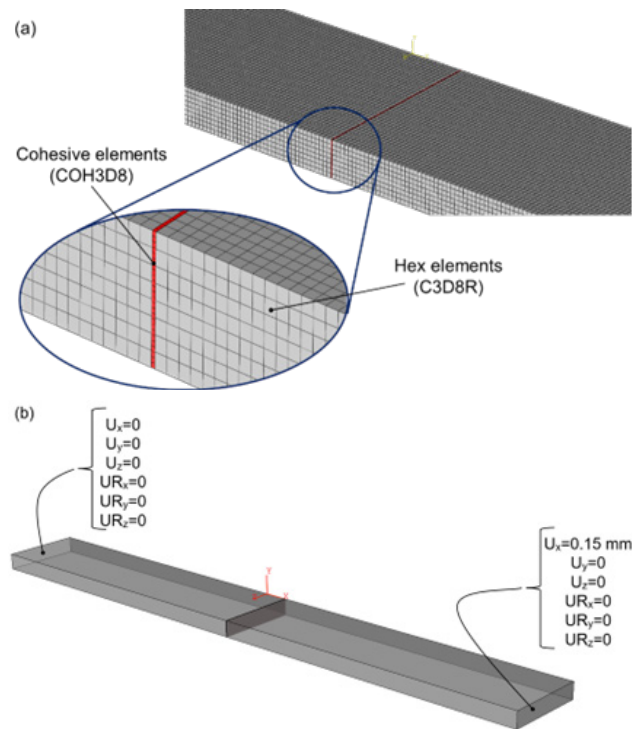
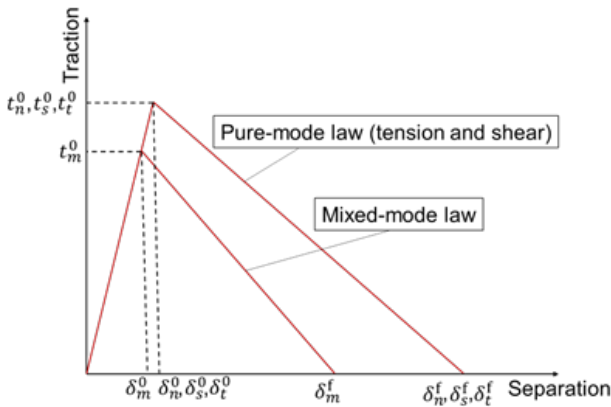


Figure 2 (a) Constructed mesh and (b) Applied boundary conditions

In this work, the adhesive's performance was determined utilizing the Cohesive Zone Model (CZM) integrated into Abaqus/Standard. CZM allows for the comprehensive definition of the fracture process through a traction-separation law, encompassing both tension and shear [1]. In the current study, a bi-linear traction-separation law was applied (Fig. 3). The first section of the traction-separation law is related to linear elastic behavior, whereas the second part refers to linear degradation [1,7]



**Figure 3** Bi-linear traction-separation law

In the current work, stress-based criterion for damage initiation (MAXS: Maximum nominal stress) was considered. According to the MAXS criterion, damage starts when the one of the maximum nominal stress ratios equals one. The damage initiation criterion, MAXS, can be expressed as follows:

$$\max \left\{ \frac{\langle t_n \rangle}{t_n^0}, \frac{t_s}{t_s^0}, \frac{t_t}{t_t^0} \right\} = 1 \quad (1)$$

where  $t_n^0$ ,  $t_s^0$ , and  $t_t^0$ , denote the maximum values of nominal stresses at the direction of normal, first shear, and second shear, respectively.  $t_n$ ,  $t_s$ , and  $t_t$  are the predicted stress values at the normal, first shear, and second shear direction, respectively. Moreover, the Macaulay bracket,  $\langle a \rangle$ , indicates that compressive stress doesn't trigger damage [12].

In CZM, total failure and separation are calculated by a damage evolution law. In the current work, the energy-based Benzeggagh-Kenane (BK) [26] fracture criterion was considered. When the critical fracture energies at the first and second shear directions are identical ( $G_{IIc} = G_{IIIc}$ ), this criterion produces more accurate results. It is expressed by:

$$G_{IC} + (G_{IIc} - G_{IC}) \left\{ \frac{G_S}{G_T} \right\}^\eta = G_C \quad (2)$$

where

$$G_S = G_{II} + G_{III}, \quad G_T = G_I + G_S \quad (3)$$

and  $\eta$  is a material parameter.  $G_I, G_{II}$ , and  $G_{III}$  denotes the normal and two shear fracture energies, respectively, whereas  $G_{IC}, G_{IIc}$ , and  $G_{IIIc}$  are their critical values [5]. In this work,  $\eta$  is chosen as 2. Properties of DP460 epoxy adhesive used in this

study for cohesive zone modeling are given in Table 2.

**Table 2** Material properties of DP460 epoxy adhesive for cohesive zone modeling [27,28]

Property	Unit	Value
$t_n^0$	MPa	32.6
$t_s^0$	MPa	28.5
$t_t^0$	MPa	28.5
$G_{IC}$	N/mm	2.56
$G_{IIc}$	N/mm	11.71
$G_{IIIc}$	N/mm	11.71

Note: Traction and critical fracture energies in the first and second shear directions are assumed to be the same ( $t_n^0 = t_t^0$  and  $G_{IIc} = G_{IIIc}$ ).

### Defect Modeling

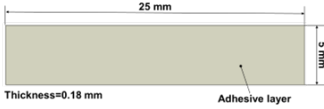
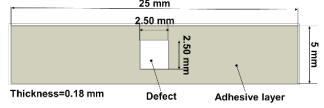
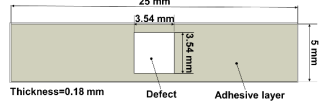
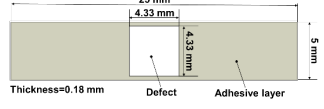
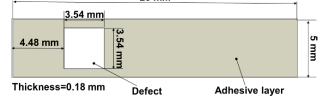

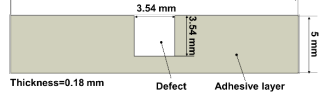

One of the main causes of the defects at the bonded region is the poor adhesive distribution, which could result from human mistakes or adherend surface imperfections. Poor adhesive distribution results in poor bonding which causes 2D (planar) and 3D (volumetric) defects [8]. In this work, the 3D (volumetric) defect was modeled as a blank volume at the adhesive. This study was mainly focused on the influences of flaw presence, volume fraction, location, and random distribution on the load carrying capacity of the butt joint. Defect volume fraction ( $V_f$ ) is the ratio of defect volume to the total adhesive volume. In order to determine the impacts of the defect existence, a bonding layer with a defect volume fraction of 0.10 and therefore a square-shaped volumetric blank in its center was modeled. The impact of defect volume fraction was investigated considering the defect volume ratio of 0.05, 0.10, and 0.15. Defect ( $V_f=0.1$ ) was shifted to the left and up to determine the effects of defect location. Regarding the influences of the defect random distribution, 3D (volumetric) defects with the dimensions of  $0.25 \times 0.25 \times 0.18$  mm<sup>3</sup> (7 pieces),  $0.50 \times 0.50 \times 0.18$  mm<sup>3</sup> (7 pieces),  $0.75 \times 0.75 \times 0.18$  mm<sup>3</sup> (6 pieces), and  $1.00 \times 1.00 \times 0.18$  mm<sup>3</sup> (7 pieces) were randomly distributed in the bonding layer. Defect details in the bonding layer are shown in Table 3.

### Verification of the Numerical Model

The numerical model was verified by comparing the experimental findings of Ref. [20]. The 3D adhesively bonded SLJ with the 0.18 mm adhesive (DP460) thickness and 3 mm adherend (AA2024-T3) thickness was modeled. The length of the adhesive layer is 12.5 mm, and the length of the adherend is 100 mm. Moreover, the width of the adherend is 25 mm. Geometric details of SLJ can be found in Ref. [20]. As in the butt joint modeling, adherend and adhesive were meshed with 70140 linear hexahedral elements of type C3D8R and 7875 linear hexahedral elements of type COH3D8. For both adhesive and adherend, the same element sizes with the butt joint were considered. Moreover, identical material properties utilized for cohesive zone modeling in the butt joints were employed for SLJ. The adherend and adhesive surfaces with different mesh structures were tied using surface-to-surface tie constraint as in the butt joint. Regarding the boundary conditions, SLJ was fixed at one end in all directions and fixed at the other end in all directions except the longitudinal

direction of adherend. A 0.5 mm uniform displacement boundary condition was applied in the longitudinal direction of the adherend.

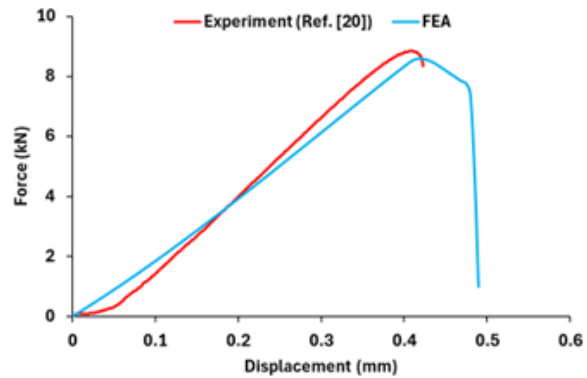
**Table 3** Graphical representation and configuration of defects in adhesive layer

Configuration	Adhesive layer with/without defect
$V_f=0.00$	
$V_f=0.05$ (Center)	
$V_f=0.10$ (Center)	
$V_f=0.15$ (Center)	
Location-1 ( $V_f=0.10$ )	
Location-2 ( $V_f=0.10$ )	
Location-3 ( $V_f=0.10$ )	
Randomly distributed ( $V_f=0.10$ )	

In this study, identical boundary conditions, mesh structures, element types, material properties, and adhesive thicknesses were employed for FE modeling of both butt joints and SLJs. Despite different failure behaviors of the two joints, given identical modeling parameters and boundary conditions, SLJ could potentially serve for FE validation. This may be related to the versatility, robustness and effectiveness of the finite element method in capturing various failure mechanisms in various joint types.

The comparison of numerical and experimental findings concerning force-displacement curves is shown in Fig. 4. A good correlation between the experimental and numerical findings were observed. The average experimental failure load and displacement were reported as  $8814 \pm 202$  N and  $0.407 \pm 0.02$  mm, respectively [20]. Based on the FEA

findings, the failure load was estimated at 8597.1 N with a relative error of 2.46%, while the displacement was calculated to be 0.419 mm with a relative error of 2.95%. The strong correlation and minimal relative discrepancies observed between the experimental and numerical outcomes for the single lap joint indicate that material properties (parameters) employed for cohesive zone modeling, element types (C3D8R and COH3D8), and element sizes are applicable for butt joint analysis as well. Furthermore, several studies [21,22,29] have also noted a strong compatibility between experimental and numerical results.

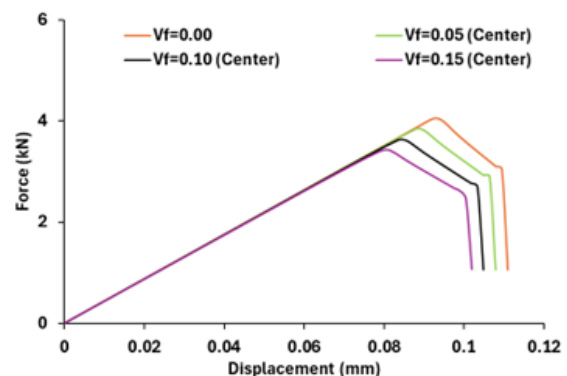


**Figure 4** Verification of numerical model

## RESULTS AND DISCUSSIONS

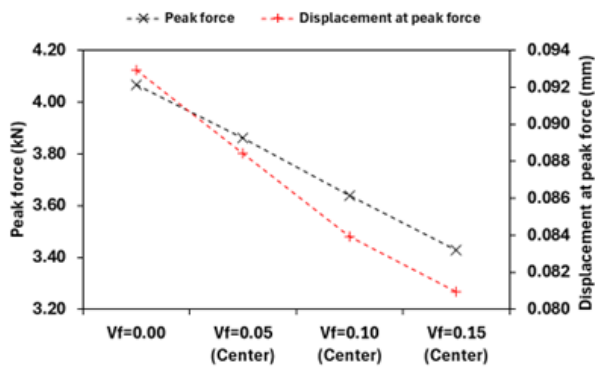
### Effect of Defect Presence and Defect Volume Fraction

Force-displacement curves for various defect volume fractions in the bonding layer are presented in Fig. 5. As shown, force-displacement curves have three linear sections. In the first section, the force exhibits a linear increase until it reaches the peak load, indicating the adhesive's elastic behavior. Subsequently, in the following section, the force linearly decreases, corresponding to the damage evolution and softening behavior of the adhesive. In the third section, there is a rapid decline in the force, corresponding to abrupt complete failure. It is clear from Fig. 5 that the elasticity of the adhesively bonded butt joint remains unaffected by the presence of defects. This provides evidence that the elasticity of the butt joint is primarily governed by the elasticity of the adherend. Because adhesive's elasticity (2077 MPa) is notably lower in comparison to that of the adherend (72400 MPa).



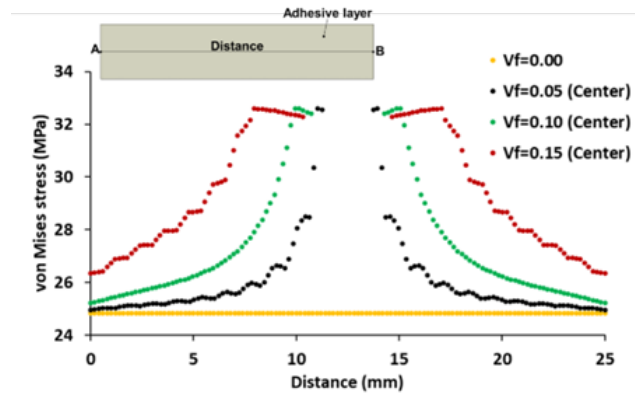
**Figure 5** Force-displacement curves for various defect volume fractions

Fig. 6 illustrates the variation in load-bearing capacity (peak force) and displacement at peak force in relation to changes in defect volume fraction. The detrimental impact of defects on the load-bearing capability of the butt joint is evident. With an increment in defect volume fraction, both the peak load and displacement at peak load decrease linearly. The introduction of a square defect at the center of the bonding layer, with volume fractions of 0.05, 0.10, and 0.15, results in peak force reductions of 4.08%, 10.56%, and 15.73%, respectively. Correspondingly, displacement at peak force decreases by 4.84%, 9.68%, and 12.91% for the same defect volume fractions. Decrease in peak load can be attributed to the decrease in bonded area. Heidarpour et al. [8] also reported a strength reduction in SLJ with the rise of 2D/3D defect size. Furthermore, according to Kumar [30], the interlaminar tensile (ILT) strength and mode-I delamination fracture energy show a linear correlation with the flaw area fraction on a critical fracture plane.

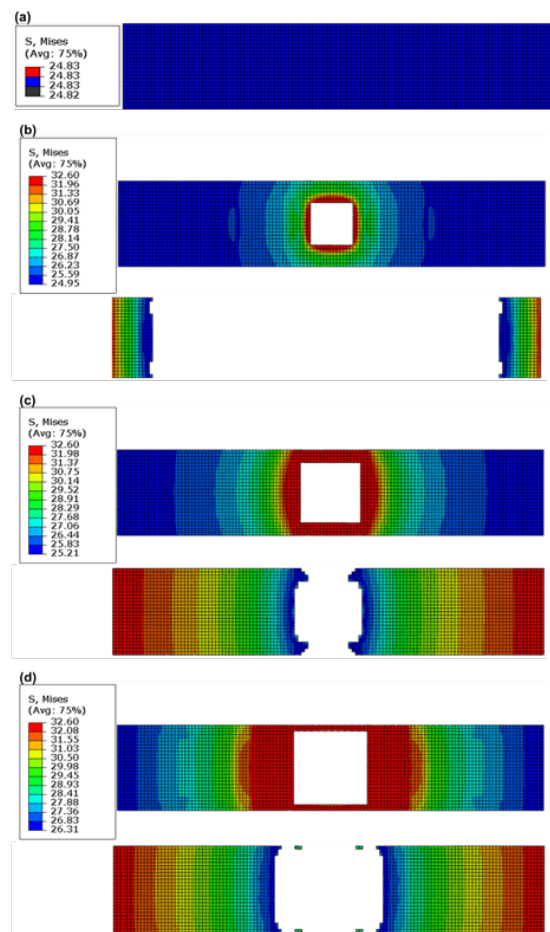


**Figure 6** Variation of peak force and displacement at peak force with the change of defect volume fraction

Fig. 7 illustrates the von Mises stress distribution along the A-B route for various defect volume fractions within the adhesive layer under a 3 kN load. Overall, there's a nonlinear increase in von Mises stress as the defect edge is approached, particularly with a sharper rise near the defect edge. The existence of a defect at the center of the adhesive layer results in approximately 31% rise in the maximum von Mises stress. Moreover, the von Mises stress at the defect edges, where the largest von Mises stress occurs, is unaffected by changes in the defect volume fractions. However, the rise of defect volume fraction results in an increase in von Mises stress at the bonding layer edges. Fig. 8 depicts the contour of von Mises stress distribution on the adhesive layer for various defect volume fractions. It is evident that as the defect volume fraction increases, the stress concentration near the defect edges becomes more severe and spreads over a larger area. Hence, the early failure of the adhesive is concentrated near the edges of the flaw as seen in Fig. 8. Conversely, in the absence of defects in the bonding layer, the initial degradation of the adhesive occurs abruptly and uniformly throughout the whole adhesive layer. Therefore, failure of adhesive layer without defect cannot be illustrated in Fig. 8.



**Figure 7** von Mises stress distribution along the path A-B for various defect volume fractions in the adhesive layer



**Figure 8** Contour of von Mises stress distribution on the bonding layer and adhesive layer initial failure for (a) Vf=0.00, (b) Vf=0.05, (c) Vf=0.10, and (d) Vf=0.15

### Effect of Defect Location

Force-displacement curves for the butt joints with a square defect positioned at various locations within the adhesive layer are illustrated in Fig. 9. Defect location is plays crucial role in the damage evolution and softening characteristics of the adhesive. Relocating the defect from the center to the left

side of the bonding layer causes a drop in the slope of the second section of the curve, indicating nearly constant-force damage evolution. However, repositioning the defect towards the upper side of the adhesive layer has little to no discernible effect on the force-displacement curve. This is probably due to the limited upward shifting capacity of the defect owing to the geometry of the butt joint.

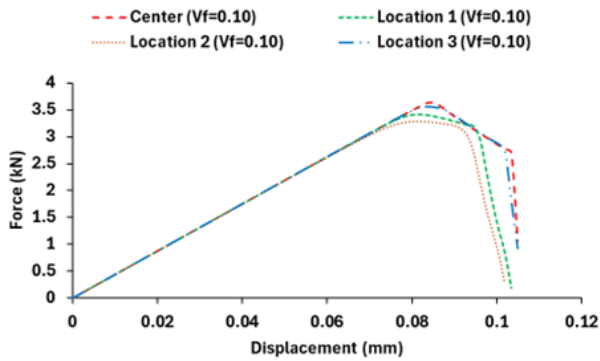


Figure 9 Force-displacement curves for various defect locations

The change of peak load and displacement at peak load depending on defect location are shown in Fig. 10. Moving the defect from the center to the left side of the bonding layer causes a drop in peak force. Specifically, shifting the defect from the center to Location 1 and Location 2 results in reductions of 6.00% and 9.79% at peak force, respectively. It is evident that defects positioned near the edges of the adhesive layer present a greater risk to the durability of butt joints. Moreover, relocating the flaw from the center to Location 3 leads to a decrease of 2.27% in the load-bearing capacity of the butt joint. These changes in the load-bearing capacity of butt joints can be attributed to the disruption of the symmetry of the bonding layer with the shifting of the flaw. Ribeiro et al. [31] carried out a numerical work to assess the influence of defects on SLJ strength. Their findings indicated that flaws close to the joint end result in a more pronounced strength drop compared to defects at the center of the joint. Chu et al. [5] similarly observed this trend, aligning with Ribeiro et al. [31], particularly for balanced SLJs constructed with identical adherends. However, it's noteworthy that the location of defects on each side of the center has different impacts on the durability of unbalanced SLJs constructed with different adherends. On the other hand, repositioning the defect from the center to Location 1 results in a 3.75% decrease in displacement at peak force, while moving it from Location 1 to Location 3 shows no impact on displacement at peak force. Furthermore, displacement at peak force remains unchanged when the defect is shifted from the center to Location 3.

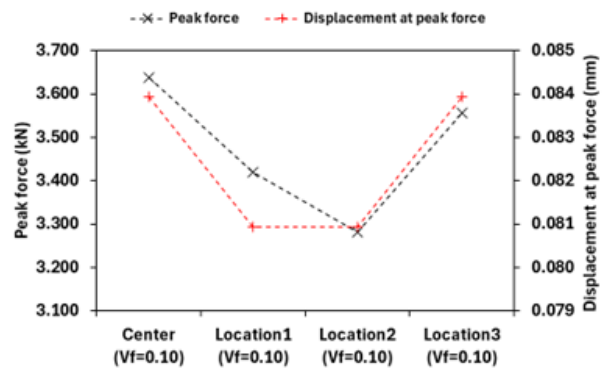


Figure 10 Variation of peak load and displacement at peak load with the change of defect location

Fig. 11 depicts the von Mises stress distribution along the A-B route for various defect positions within the adhesive layer for the case of 3 kN loading. There is no change in the von Mises stress distribution when the defect is moved to upper side of the bonding layer. However, as the defect is shifted from the center to the left side, von Mises stress at the left side of the bonding layer rises whereas von Mises stress at the right side of the bonding layer drops. At the left edge of the adhesive, there is an increase of 11.81% and 25.19% for Location 1 and Location 2, respectively, while experiencing a decrease of 4.56% and 20.64%, respectively, at the right edge. Regarding the maximum von Mises stress, altering the defect location does not affect its value. Von Mises stress fields on the adhesive layer for various defect positions are illustrated in Fig. 12. Stress concentrations occur at the edges of the defects, as evidenced by Fig. 12. Moreover, as the flaw is moved from the center to the left side, the stress concentration near the defect edges becomes more severe and spreads over a larger area. The adhesive failure starts at the left edge of the bonding layer, correlating with repositioning the defect towards the left side, as depicted in Fig. 12. Similarly, relocating the defect to the upper side leads to the onset of adhesive failure at the upper edge of the bonding layer.

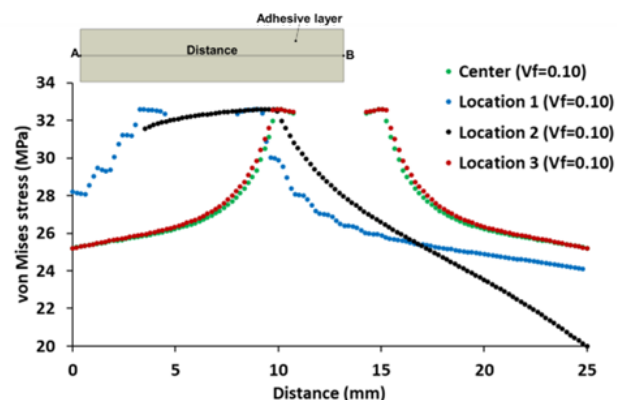
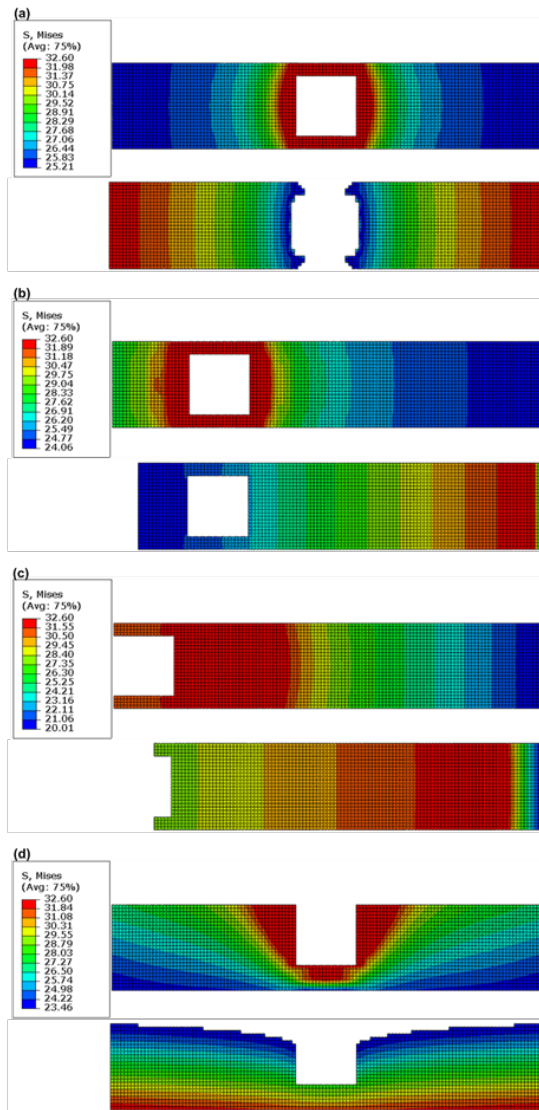


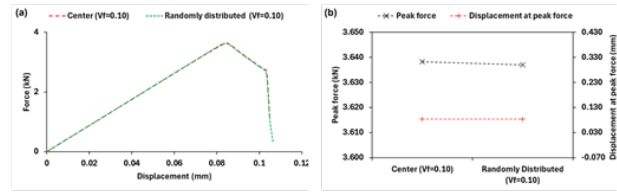
Figure 11 von Mises stress distribution along the path A-B for various defect locations in the adhesive layer



**Figure 12** Contour of von Mises stress distribution and adhesive failure on the bonding layer for various defect locations (a) Center ( $V_f=0.10$ ), (b) Location 1 ( $V_f=0.10$ ), (c) Location 2 ( $V_f=0.10$ ), and (d) Location 3 ( $V_f=0.10$ )

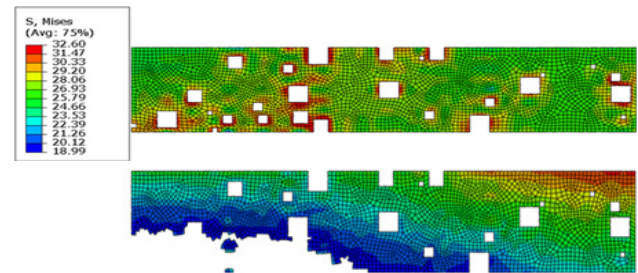
**Effect of Defect Random Distribution**

Fig. 13 displays the force-displacement curves and peak load and displacement at peak load for the butt joints with a defect located at the center of the bonding layer and defects randomly distributed in the adhesive layer. It is evident that the random distribution of defects does not exert any discernible influence on the durability of butt joints. The random distribution of flaws creates approximately equal defect areas on both sides of the symmetry planes (XY and XZ planes). Consequently, an adhesive layer with an almost symmetrical structure is formed. This roughly symmetrical structure explains why the load-bearing capacity remains unchanged.



**Figure 13** (a) Force-displacement curves and (b) peak load and displacement at peak load for the butt joints containing a defect at the center of the bonding layer and defects randomly distributed in the bonding layer

Fig. 14 depicts the von Mises stress distribution on the bonding layer under a 3 kN loading condition, considering the presence of randomly distributed defects. Localized stress concentrations arise at the edges of defects, and adhesive damage begins in the area where the defects are concentrated.



**Figure 14** Contour of von Mises stress distribution and adhesive failure on the bonding layer with randomly distributed defects

**CONCLUSION**

This study scrutinizes the influence of defect presence, defect volume fraction, defect location, and random distribution of defects in the bonding layer on the load-carrying capacity of the butt joint. A FE model in Abaqus/Standard was created and the butt joint was exposed to uniaxial tensile load while exclusively considering only cohesive failure. Defect presence has a great effect on the durability of the butt joint. Increasing the defect volume fraction within the adhesive layer causes a reduction in both peak force and displacement at peak force. Every 5% increment in defect volume fraction in adhesive layer causes a 5% drop in load-bearing capacity of the butt joint. As the defect volume fraction increases, stress concentration near the defect edges becomes more pronounced and extends over a wider region. Therefore, adhesive failure first initiates at the defect edges. Regarding the defect location, shifting the defect from the center to the left side of the bonding layer causes a reduction in peak load and displacement at peak load and the onset of the adhesive failure at the left edge of the adhesive. However, both peak force and displacement at peak force do not alter as the defect is moved to the upper side of the adhesive. The load-carrying capability of butt joints remains unaffected by the random distribution of flaws in the adhesive layer. Considering the widespread use of adhesively bonded joints, the findings of this study significantly contribute to the current knowledge. The results obtained can be utilized by researchers and industry professionals across a broad range of sectors, from automotive to aerospace.



## Acknowledgement

The author received no financial support for the research, authorship, and/or publication of this article.

## References

- Moya-Sanz EM, Ivañez I, Garcia-Castillo SK. Effect of the geometry in the strength of single-lap adhesive joints of composite laminates under uniaxial tensile load. *Int J Adhes Adhes.* 2017;72:23–9.
- Shishesaz M, Hosseini M. Effects of joint geometry and material on stress distribution, strength and failure of bonded composite joints: an overview. *J Adhes.* 2020;96:1053–121.
- Geleta TN, Woo K, Cairns DS, Samborsky D. Failure behavior of inclined thick adhesive joints with manufacturing defect. *J Mech Sci Technol.* 2018;32:2173–82.
- Sadeghi MZ, Gabener A, Zimmermann J, Saravana K, Weiland J, Reisinger U, et al. Failure load prediction of adhesively bonded single lap joints by using various FEM techniques. *Int J Adhes Adhes.* 2020;97:102493.
- Chu Y, Sun L, Zhan B, Yang X, Zhang C, Huang W. Static and dynamic behavior of unbalanced bonded joints with adhesion defects in automotive structures. *Compos Struct.* 2019;226:111234.
- Shang X, Marques EAS, Machado JJM, Carbas RJC, Jiang D, da Silva LFM. Review on techniques to improve the strength of adhesive joints with composite adherends. *Compos Part B Eng.* 2019;177:107363.
- Rocha RJB, Campilho RDSG. Detailed investigation of the analysis conditions in the evaluation of bonded joints by cohesive zone models. *J Phys Conf Ser.* 2017;843:012002.
- Heidarpour F, Farahani M, Ghabazi P. Experimental investigation of the effects of adhesive defects on the single lap joint strength. *Int J Adhes Adhes.* 2018;80:128–32.
- Guo W, Chen P, Yu L, Peng G, Zhao Y, Gao F. Numerical analysis of the strength and interfacial behaviour of adhesively bonded joints with varying bondline thicknesses. *Int J Adhes Adhes.* 2020;98:102553.
- Kanani AY, Hou X, Laidlaw R, Ye J. The effect of joint configuration on the strength and stress distributions of dissimilar adhesively bonded joints. *Eng Struct.* 2021;226:111322.
- Elhannani M, Madani K, Chama Z, Legrand E, Touzain S, Feaugas X. Influence of the presence of defects on the adhesive layer for the single-lap bonded joint—Part II: Probabilistic assessment of the critical state. *Aerosp Sci Technol.* 2017;63:372–86.
- Majid J-O, Mohammad Reza MS. Investigation of Defect Effects on Adhesively Bonded Joint Strength Using Cohesive Zone Modeling. *Strojnícky Cas – J Mech Eng.* 2018;68:5–24.
- Luo G, Chai C, Liu J, Xiao Y, Chen Y, Xu F. Investigations on the Mechanical Properties of Composite T-Joints with Defects under Bending Loading. *Sustainability.* 2022;14:16609.
- Xu W, Wei Y. Strength analysis of metallic bonded joints containing defects. *Comput Mater Sci.* 2012;53:444–50.
- Elhannani M, Madani K, Legrand E, Touzain S, Feaugas X. Numerical analysis of the effect of the presence, number and shape of bonding defect on the shear stresses distribution in an adhesive layer for the single-lap bonded joint; Part I. *Aerosp Sci Technol.* 2017;62:122–35.
- Dai T, Yang Y, Dai H-L, Hu Z. Interfacial stress analysis of a CFRR-metal adhesively bonded joint with/without defect under hygrothermal environment. *Appl Math Model.* 2019;67:357–77.
- Fame CM, Wu C, Feng P, Tam L. Numerical investigations on the damage tolerance of adhesively bonded pultruded GFRP joints with adhesion defects. *Compos Struct.* 2022;301:116223.
- Kumar RS. Mode-II interlaminar fracture of composite materials in the presence of randomly distributed defects. *Int J Fract.* 2021;231:201–21.
- Ribeiro FMF, Campilho RDSG, Carbas RJC, da Silva LFM. Strength and damage growth in composite bonded joints with defects. *Compos Part B Eng.* 2016;100:91–100.
- Sahin R, Akpınar S. The effects of adherend thickness on the fatigue strength of adhesively bonded single-lap joints. *Int J Adhes Adhes.* 2021;107:102845.
- Çalık A, Yıldırım S. An investigation on the effect of parallel slot in bi-adhesive single lap joints with spew fillet. *J Eng Res.* 2015;3:36.
- Çalık A, Akpınar S. Dört Nokta Eğme Yüküne Maruz Yapıştırma Bağlantılarında İç Kademenin Bağlantı Hasar Yüküne Etkisi: Deneysel ve Sayısal Analiz. *Osman Korkut Ata Üniversitesi Fen Bilim Enstitüsü Derg.* 2022;5:1128–40.
- Liao L, Huang C, Sawa T. Effect of adhesive thickness, adhesive type and scarf angle on the mechanical properties of scarf adhesive joints. *Int J Solids Struct.* 2013;50:4333–40.
- Chen P, Guo W, Zhao Y, Li E, Yang Y, Liu H. Numerical analysis of the strength and interfacial properties of adhesive joints with graded adherends. *Int J Adhes Adhes.* 2019;90:88–96.
- Liao L, Huang C. Numerical analysis of effects of adhesive type and geometry on mixed-mode failure of adhesive joint. *Int J Adhes Adhes.* 2016;68:389–96.
- Benzeggagh ML, Kenane M. Measurement of mixed-mode delamination fracture toughness of unidirectional glass/epoxy composites with mixed-mode bending apparatus. *Compos Sci Technol.* 1996;56:439–49.
- Kanar B, Akpınar S, Avinc Akpınar I, Akbulut H, Ozel A. The fracture behaviour of nanostructure added adhesives under ambient temperature and thermal cyclic conditions. *Theor Appl Fract Mech.* 2018;97:120–30.
- Kazaz I, Akpınar S, Ozel A. The effects of thermal cycle and nanostructure reinforcement on the shear load in adhesively bonded joints. *Mech Adv Mater Struct.* 2020;27:1627–38.
- Akpınar S, Çalık A. Dört Noktalı Eğme Testi Altında Yapıştırıcı ile Birleştirilmiş Bindirme Bağlantısının Deneysel ve Sonlu Elemanlar Analizi. *Çukurova Üniversitesi Mühendis Fakültesi Derg.* 2021;36:649–57.
- Kumar RS. Effects of randomly distributed defects on Mode-I interlaminar fracture of composite materials. *Eng Fract Mech.* 2021;248:107699.
- Ribeiro FL, Borges L, d'Almeida JRM. Numerical stress analysis of carbon-fibre-reinforced epoxy composite single-lap joints. *Int J Adhes Adhes.* 2011;31:331–7.